Laser induced fluorescence and electron paramagnetic resonance for the characterization of aromatic species and resonant stabilized radicals involved in the soot nucleation process

J Elias, A Faccinetto, H Vezin, X Mercier

Laser induced fluorescence and electron paramagnetic resonance for the characterization of aromatic species and resonant stabilized radicals involved in the soot nucleation process

J. Elias[1,2], A. Faccinetto[1], H. Vezin[3], X. Mercier[1*]

[1]PC2A, Université Lille, CNRS, UMR 8522, France
[2]French Environment and Energy Management Agency, France
[3]LASIRe, Université Lille, CNRS, UMR 8516, France

Abstract

This work presents the analysis of *in situ* laser-induced fluorescence (LIF) and *ex situ* electron paramagnetic resonance (EPR) measurements performed in a sooting atmospheric methane co-flow diffusion flame stabilized on a Gülder-type burner. We implemented these techniques in order to obtain information on the species involved in the nucleation processes of soot particles in flames. The LIF experiments were performed using excitation-emission matrices (EEM) to study the spectroscopic properties of the compounds formed in the flame. The analysis of these images, carried out by means of EEM arrays of pure PAHs, allowed the identification of a type of intermediate species characterized by optical properties distinct from PAHs and soot. The EPR data were obtained using various methods (EPR imaging, continuous wave EPR and pulsed wave EPR) allowing the localization of persistent radicals along the flame height, their quantification and a partial analysis of their structure. A remarkable correspondence is found between the concentration profile of persistent radicals and that of the fluorescent intermediates in the visible range, determined from the EEM arrays. Finally, the analysis of hyperfine interactions by ^{1}H hydrogen, ^{13}C carbon HYSCORE spectroscopy indicates the presence of aromatic coronene-sized radical structures and highly branched PAH clusters in nascent soot.

Introduction

Particulate emission during combustion processes are the subject of special attention notably because of their potential involvement both in climate change and health pathologies going from cardiovascular diseases to lung cancer and respiratory allergies [1]. Although the soot formation in combustion has been the subject of numerous research projects for more than forty years, a number of questions still remain open. In particular, the nucleation step, characterized by the transformation of gaseous PAHs into soot particles, encompasses a number of uncertainties regarding both on the physicochemical mechanisms and the species involved in this process.

While PAHs are well known to be strongly interconnected to the formation of soot in flames [2], recent works, both experimental and theoretical, highlight the possible involvement of resonance-stabilized radical (RSR) aromatic compounds in these mechanisms [3,4]. In that context we carried out a series of experiments in a laminar sooting diffusion flame by using laser induced fluorescence (LIF) and electron paramagnetic resonance (EPR). The LIF experiments were performed using excitation-emission matrices (EEM). The analysis of these images, carried out by means of EEM arrays of pure PAHs, allowed a partial identification of the aromatic species formed in the flame based on their optical properties.

[1]The EPR data were obtained using various methods (EPR imaging, continuous wave EPR and pulsed wave EPR) allowing the localization of the persistent radicals along the flame height, their quantification and a partial analysis of their structure. This innovative approach provides valuable information for the characterization of the interconnection of PAHs and persistent radicals notably at the onset of the soot formation in the flame, as well as some structural information about the aromatic unit contained in nascent soot.

Experimental

Burner and sampling probe setup

In this work, measurements were carried out on a 120 mm height laminar diffusion methane flame stabilized on a Gülder-type burner at atmospheric pressure [5]. This burner consists of a central injector supplied with 0.52 L min^{-1} of methane and surrounded by 86.6 L min^{-1} air flow (standard p and T). The flame is characterized by a partially stratified distribution of PAHs and soot through the centerline that allows sampling at different heights above the burner (HAB) to monitor the steps of soot formation.

Samples were extracted from the flame using a quartz dilutive microprobe ending with a thin tip in which a 250 µm diameter orifice was obtained by abrasion and inserted radially into the flame. The small orifice allowed maintaining a constant pressure difference (≈500 mbar) between the flame and the probe during the sampling. Extracted species were diluted by nitrogen (0.5-5.0 L min^{-1}) in the mixing chamber at the tip of the probe to reduce the collision probability in the sampling line and limit the reactivity. The collected species were deposited on glass microfiber filters installed in a sample holder system downstream the probe. An automatic pressure regulation system was located further downstream the

* Corresponding author: xavier.mercier@univ-lille.fr

sample holder and consisted of a HEPA filter, a Pfeiffer EVR116 regulation valve and a pumping unit. The sampling time for the diffusion flame was set to 3 min per sample.

LIF setup

The experimental setup is the same as the one described in [6], so only the main details will be given here. The excitation source used for the LIF analyses consists of a Nd:YAG laser (Quanta-ray, Spectra Physics) generating laser pulses at 1064, 532 and 355 nm (6 ns pulse width, 10 Hz) which are mixed and used to pump an optical parametric oscillator (OPO - premiScan-ULD/240, GWU-Lasertechnik) allowing the generation of tunable laser pulses over a wide spectral range (210 nm to 2 μm).

The experimental study carried out with this setup enabled the determination of the excitation-emission matrix (EEM). To do this, measurements of fluorescence emission spectra obtained for different excitation wavelengths were recorded at different HAB in the flame. 14 excitation wavelengths were selected in the UV/visible range for the determination of the EEM (215, 220, 230, 240, 250, 265, 280, 290, 370, 405, 488, 532, 594, and 658 nm). A variable energy attenuator was positioned before the flame to control the energy of the laser beam. The purpose of this control was mainly to limit the laser energy used for LIF measurements in order to be in the linear fluorescence energy regime and to avoid the triggering of the laser induced incandescence (LII) process emitted by soot particles at high HABs. The beam was focused at the center of the flame with a spherical lens (f = 300 mm) to increase the photon density and the number of molecules excited in the flame and to perform measurements with an adequate spatial resolution. The diameter of the laser beam at the focus point was estimated to be around 500 μm. A calorimeter was installed behind the flame to control the pulse power.

The emitted fluorescence was collected at right angle with two spherical lenses (f = 200 mm and 50 mm diameter). The collected fluorescence was transmitted, by means of a 1.25 mm diameter bundle consisting of a set of 19 optical fibers of 200 μm diameter (model LG-455-020), to a spectrometer (IHR320, Jobin Yvon) equipped with a 100 line/mm grating blazed at 450 nm. The spectrometer was coupled to a PI-MAX2 Roper Scientific ICCD (Intensified Charge-Coupled Device) camera for the acquisition of fluorescence spectra, featuring an RB (red-blue) Gen II intensifier interfaced to a PC using Winspec32® software. To limit interfering signals related to laser scattering, we used different high-pass filters at 280 nm, 295 nm and 305 nm respectively for excitation wavelengths below 265 nm, 280 nm, and 290 nm, and notch filters centered at the excitation wavelengths for wavelengths above 370 nm. These filters were used to suppress the intense scattering signal generated by the excited beam from the fluorescence emission spectra at wavelengths 370 nm, 405 nm, 488 nm, 532 nm, 594 nm, and 658 nm. Two positions of the spectrometer were defined to cover the entire PAH fluorescence emission spectral range from 280 to 840 nm. The spectra were recorded every 2.5 mm at low HAB (10-20 mm) and then every 5 mm up to 90 mm HAB. Finally, for all the studied HABs, the measured spectra were corrected from the signal coming from the natural emission of the flame (continuous emission) and from the transmission function of the whole detection system (determined separately thanks to a calibrated halogen/deuterium lamp).

EPR setup

Pulsed EPR measurements were carried out at X-band (9 GHz) at 5 K with a Bruker Elexsys E580 spectrometer equipped with a helium flow cryostat. Concentration of organic radicals were derived from the CW and echo detected field sweep experiments ($\pi/2–\tau–\pi–\tau$) where the pulse lengths were set to 32 ns for the π pulse and 16 ns for the $\pi/2$ pulse with τ = 136 ns. $\pi/2$ and π represent the angles of rotation of the electron magnetization and τ the time delay between pulses.

Hyperfine interactions, i.e. interactions between the electron spin of the radical and neighboring nuclear spins, were measured using the two-dimensional four-pulse electron spin echo envelope modulation (ESEEM) ($\pi/2–\tau–\pi/2–t_1–\pi–t_2–\pi/2–\tau$). This technique is also referred to as HYperfine Sublevel CORrElation spectroscopy (HYSCORE) whereby a π pulse is intercalated between two $\pi/2$ microwave pulses and the echo intensity is measured after the fourth pulse at fixed τ. The echo intensity exhibits modulations due to the presence of magnetic dipolar interactions between the unpaired electron of the radical and neighboring nuclear spins and is measured by varying t_1 and t_2 at fixed τ. This two-dimensional set of echo modulations gives, after Fourier transformation, a two-dimensional HYSCORE spectrum, which is represented by contour plots where the corresponding nuclear frequencies are obtained. This technique allows the detection of elements with non-zero nuclear spins such as ^{1}H and ^{13}C and the evaluation of the H/C ratio.

A continuous wave EPR X-band Bruker Elexsys E580 spectrometer operating at around 9 GHz at room temperature was used to record both continuous EPR spectra and 2D spatial images. The microwave power supplied into the resonator where the sample was placed and the modulation amplitude were set to 10 mW and 4 G respectively. The signal was recorded with a field-of-view of 25 mm and a gradient strength of 175 G cm^{-1}. The size of 2D YZ images was 512 × 512 pixels resulting in a pixel size of 0.05 mm. The image processing involved deconvoluting the acquired projections under a magnetic field gradient from the reference signal recorded without gradient. Both signals were back-projected using Fourier transformation, giving the spatial distribution of organic radicals in the samples.

EEM results and analysis

As introduced above, the fluorescence experiments have been carried out by using excitation-emission matrix (EEM). This methodology allows a richer exploitation of the LIF data and a finer identification of the spectral structures of the species formed in the flame than common fluorescence spectroscopy based on the use of a specific excitation wavelength.

In order to extract relevant information from the EEM characterizing the PAHs and soot precursors formed in flame, we first built reference EEM from known spectra of several pure PAHs. The choice of the PAHs constituting this database, necessarily limited and arbitrary, was based on the LIF data (excitation and emission spectra) of pure PAHs (potentially formed in sooting flames) available in the literature [7]. We considered a set of 15 PAHs ranging from naphthalene (2 aromatic rings) to coronene (7 aromatic rings) chosen among the most commonly reported PAHs in the literature and representative of all the aromatic families and structures commonly accepted as having a potential involvement in the soot formation mechanisms.

Example of a few EEM for pure PAHs are reported in fig.1. This figure highlights that PAHs are characterized by intense absorption bands in the UV region (200-300 nm), which shift and broaden to longer wavelengths as the size and number of aromatic rings of PAH increases. The corresponding fluorescence emission spectra of these species are characterized by emission bands in the 300-450 nm spectral range. As it can be seen in the figure, only a limited number of PAHs, likely to be formed in flames and consisting of 4 or more aromatic rings, have absorption bands above 400 nm. No PAHs up to coronene display significant absorption bands above 450 nm.

From these EEM, we can therefore state that any features appearing outside a spectral zone roughly comprised between 200 and 400 nm in excitation and 350 and 500 nm in emission, is unlikely to be a PAH spectral signature. As discussed later, although the separation of the different contributions of PAHs in the flames remains delicate, the EEM methodology offers the advantage of allowing the distinction between spectral features characteristic of PAHs and signals related to the formation of other aromatic compounds.

The EEM built from the fluorescence emission spectra recorded in the flame as a function of HAB (from 10 to 90 mm) are shown in fig.2. It should be noted that the areas with no emission signal appearing on these images around specific visible wavelengths (dark blue "holes" on the EEM matrices) indicate the use of notch filters implemented to suppress the intense scattering peaks in the visible due to laser excitation.

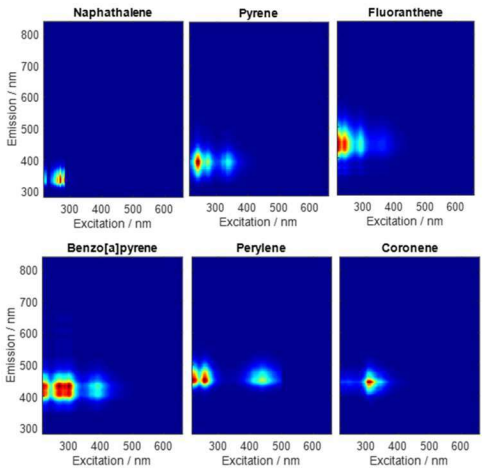

Figure 1: EEM matrices of reference PAHs at 1750 K

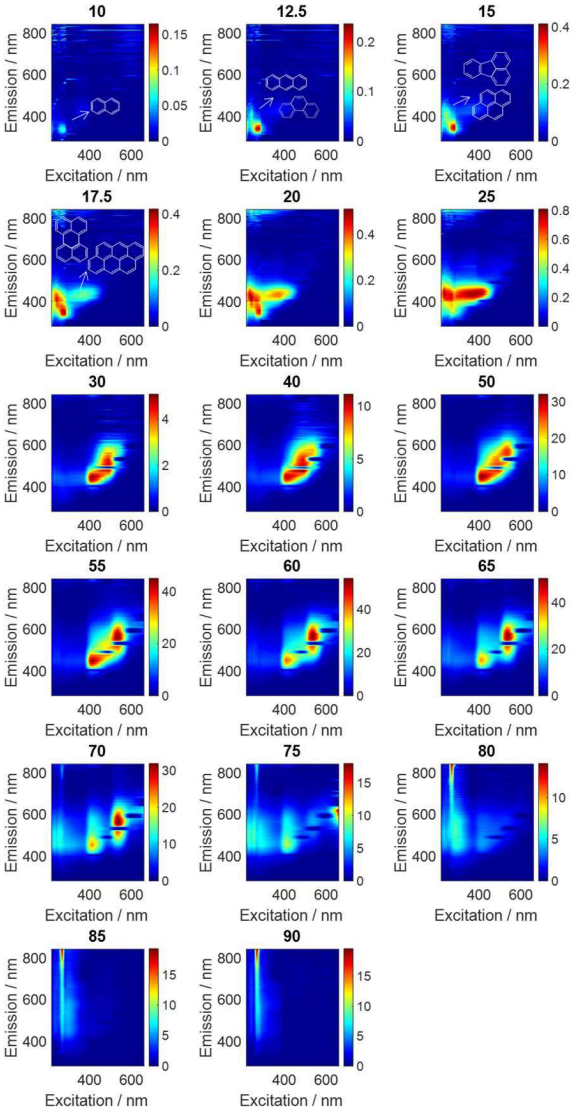

Figure 2: EEM of the methane diffusion flame as a function of HAB from 10 to 90 mm.

As it can be seen in Fig.2 for the first two HABs (10 and 12.5 mm HAB in the flame) in the condensable gas zone, spectral structures are observed showing a main contribution attributable to naphthalene. At 12.5 mm HAB, we also note the appearance of additional contributions characteristic of the formation of larger PAHs (3 cycles) such as phenanthrene and anthracene. From 15 mm, the contribution of species with 4 aromatic rings such as pyrene and fluoranthene can be distinguished, characterized in particular by the appearance of spectral features around 400 nm in emission. The EEM at 17.5 mm and 20 mm show the contributions of species with 5 and 6 aromatic rings such as benzo[a]pyrene, perylene and potentially anthanthrene. At 25 mm HAB, we observe the progressive decrease of the spectral components characteristic of small PAHs (2 and 3 aromatic rings) compared to the spectral components of moderate sized PAHs (4, 5 and 6 aromatic rings).

Above 30 mm, a very intense spectral feature is observed in the visible range which cannot be attributed to the fluorescence of the 15 reference PAHs. This signal intensity increases with the HAB to reach its maximum in the nucleation zone (determined elsewhere [6]) around 60 mm HAB. It should be noted that the UV signal of the PAHs is still present in the EEM of the flame but its visualization is overwhelmed by the intensity of the visible signal (about 4 times higher than the UV emission signal). This signal then becomes the major spectral component observed between 30 and 70 mm. It seems to be globally constant in size over this area (no growth or spectral shifts).

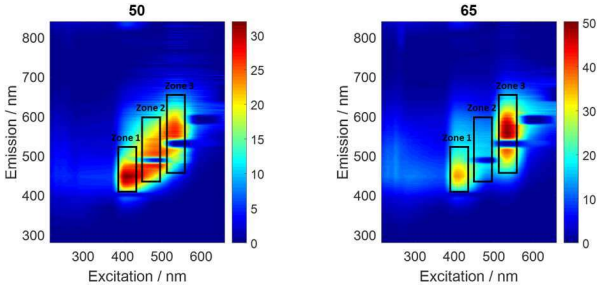

Figure 3: Structuring of the visible spectral component into 3 zones at 50 and 65 mm HAB.

On the other hand, one can distinguish a structuring of this component which might be roughly divided in 3 zones whose intensities evolve differently with the HAB as indicated in Fig.3. The first structure defined between 350 and 450 nm probably contains an overlap with the spectral components of PAHs with 4 and more aromatic rings. However, the contributions observed at higher excitation wavelengths highlight the involvement of other photophysical processes than simply PAH fluorescence and therefore probably characteristic of species of different nature. Hence, if the interpretation of the spectral structures observed lower in the flame in the UV range are easily attributable to the fluorescence of PAHs in the gas phase, the interpretation of the signals observed in the visible range appears more complex. As previously mentioned, we have taken care to use low laser energies to avoid initiating any LII process of soot particles present in the flame. The fluorescence emission spectra are therefore clearly characteristic of the emission of species quite distinct from soot particles. Moreover, the observed signals characterizing these absorbing and fluorescent species in the visible range are mainly formed in the nucleation zone and disappear in the oxidation zone where the soot volume fraction determined by LII measurements reaches its maximum (around 80 mm). Although these signals have already been suggested to be due to large PAHs or dimers of PAHs [6], we proved here that the first hypothesis cannot explained the observed signal for spectroscopic reasons, while the second one, although coherent with the observed fluorescence signal obtained upon UV excitation wavelength, cannot fully explained the fluorescence bands measured upon visible excitation wavelength. Hence, the exact origin of these intense signals mainly observed in the nucleation region, while remaining uncertain, cannot be attributed to gaseous PAHs or soot particles.

EPR results and analysis

Fig.4 compares the EPR imaging with the pictures of the samples taken from the flame at different HAB.

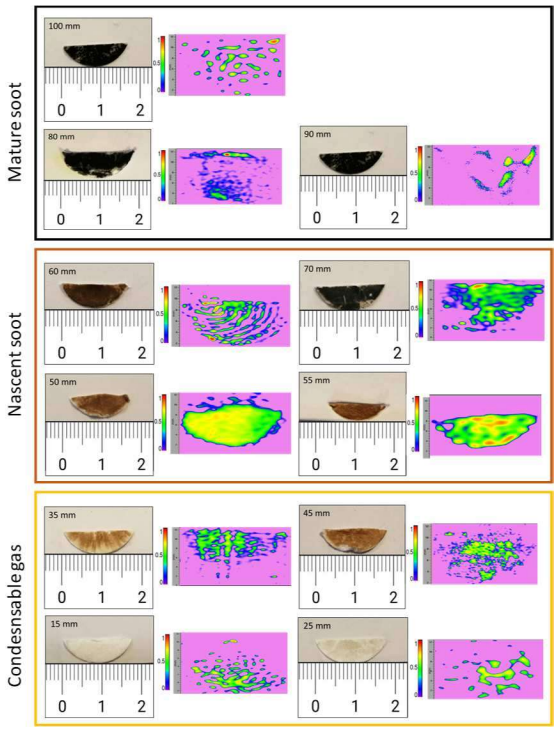

Figure 4: pictures of the collected samples at different HAB and corresponding EPR images (512 × 512 image resolution, 0.05 mm pixel size). The colormap represents the spin concentration in relative unit, increasing from purple to red.

The EPR images characterize the spatial distribution of the spin density of the carbon radicals. As it can be seen, samples in 15-45 mm HAB are characterized by highly heterogeneous EPR images,

with small and scattered signal islands that become larger and denser with the increasing HAB. We observe on the pictures of the samples that the increase of the EPR signal is associated to the appearance of a deposit of brownish matter. From 60-70 mm HAB, the color of the deposited matter transitions from brown to black characteristic of soot and corresponds to the appearance of incandescent soot particles in the flame [6]. Above 70 mm HAB, the signal intensity in EPR images begins to decline and small and scattered signal islands appear again.

Following these experiments, we reported in fig.5 the evolution of the spin density found on the sample against the visible LIF signal intensity. As it can be seen, the determined spin concentration is found to be well correlated to the relative concentration of soot precursors measured *in situ* in the flame by optical methods (laser induced fluorescence [6]). Although the concentration of the individual fluorophores cannot be determined, this general correlation suggests that persistent radicals in the flame extracts are related to the species fluorescing in the flame.

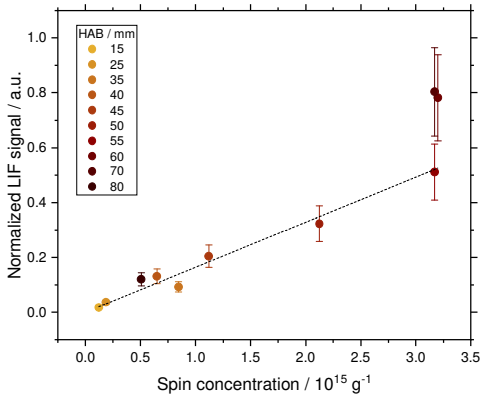

Figure 5: normalized laser induced fluorescence signal (532 nm excitation) against spin concentration (datapoints) and linear fit (dashed line, $R^2 = 0.8943$).

In addition, we carried out some pulsed EPR experiments with the same samplings. The analysis of the hyperfine interaction provides information on the nature of the chemical bonds, the structure of the electron ground state and the electron-nucleus distance, and thus gives direct information on the structure of the radicals. These data can be determined from the analysis of the two-dimensional HYSCORE spectrum corresponding to the resulting two-dimensional set of echo modulations after Fourier transform. In the case of alkylated polyaromatic radicals, ^{1}H HYSCORE spectra contain important chemical information on the nature of C-H bonds [9]. Three types of hydrogens can be distinguished in the molecular structure depending on their distance from the edge carbon atoms. First, aromatic hydrogens (directly bound to aromatic carbons, H_a) are characterized by a significant dipolar interaction T in addition to the isotropic interaction A_{iso} resulting in peaks and ridges that are positively shifted from the anti-diagonal and exhibiting a typical "horn shape". Second, benzylic hydrogens (bound to aliphatic carbons next to an aromatic system, H_b) are characterized by a hyperfine interaction dominated by the isotropic coupling term A_{iso}, with only a weak dipolar contribution T leading to pairs of spots along an axis $\upsilon_1 = - \upsilon_2$ crossing the diagonal $\upsilon_1 = \upsilon_2$, with a splitting equal to A_{iso}. Finally, distant hydrogens (bound to aliphatic carbons next to other aliphatic carbons, H_d) are characterized by a weak dipolar interaction giving a central peak along the diagonal $\upsilon_1 = \upsilon_2$ at the nuclear frequency of ^{1}H ν = 14.5 MHz. These HYSCORE spectra might therefore advantageously be used to obtain information on the structure of polyaromatic radical contained in nascent soot.

The evolution of the HYSCORE spectra for selected HABs is reported in fig.6. This figure shows that the hyperfine interactions of ^{1}H are all contained in the quadrant υ_1 and $\upsilon_2 > 0$, which is characteristic of weak couplings between the unpaired electron and the neighboring nuclei. Second, the HYSCORE spectrum of the condensable gas shows the presence of ^{13}C (3.7 MHz) and ^{14}N (4.6 MHz), while no signal of ^{1}H (expected at 14.5 MHz) is observed. The contribution of ^{1}H only appears above 35 mm HAB and keeps increasing up to 70 mm HAB. A typical HYSCORE spectrum characteristic of this region and recorded at 70 mm HAB is reported in fig.6. In the mature soot above 80 mm HAB, the signal of ^{1}H suddenly disappears and a change in the shape of the carbon signal, representative of the signature of PAH macrocycles (graphitized soot) is clearly visible in fig.6.

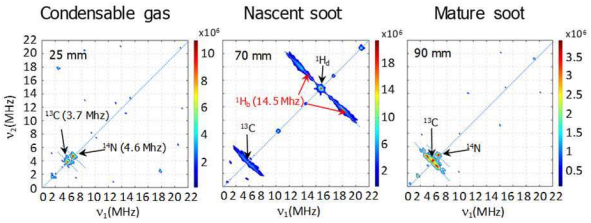

Figure 6: HYSCORE spectra of soot sampled at 25, 50, 70 and 90 mm in the central axis of the flame. Nascent soot is detected above 55-60 mm HAB.

These results are consistent with the echo detected field sweep measurement results and highlight for ^{1}H that the unpaired electron interacts with nuclear spins by two different hyperfine interactions. The intense peak in the $\upsilon_1 = \upsilon_2$ diagonal is characteristic of the hyperfine interaction with distant ^{1}H and thus of aliphatic side chains, while the broad ridges on both sides of this central peak represent the hyperfine interaction with benzylic ^{1}H. It is worth noticing that the typical spectrum of aromatic ^{1}H is never observed for any sample. This strongly suggests that in the radicals in the soot samples many aromatic hydrogens have been substituted with aliphatic side chains, the sources of benzylic and distant hydrogens. By analogy

with insoluble organic matter constituted of highly branched aromatic clusters linked by short and branched aliphatic chains [10–12], the elongated shape of the signal ridge of benzylic hydrogens and the dominant signal of distant hydrogens in the HYSCORE spectra are indicative of branched aromatic radicals. Also interesting to note are the drastic drop of the ^{1}H signal and the change of shape of the ^{13}C signal above 80 mm. The evolution of the HYSCORE spectra highlights major differences in the nature of the radicals in nascent and mature soot and therefore appears to be an indicator of the soot degree of maturation. In particular, the substituted aromatic radicals prominent in nascent soot are completely absent in mature soot.

Finally, we compared in fig.7 the HYSCORE obtained for our nascent soot and a specific coke of determined identity trapped in a zeolite. As it can been seen, these two pictures share several similarities. First, the ^{1}H ridges (delimited by the blue dotted lines) characterizing benzylic hydrogens appear slightly shifted from the central signal at 14.7 MHz of distant hydrogens. Second, the shape of the ridge of the ^{13}C signal is close to nascent soot.

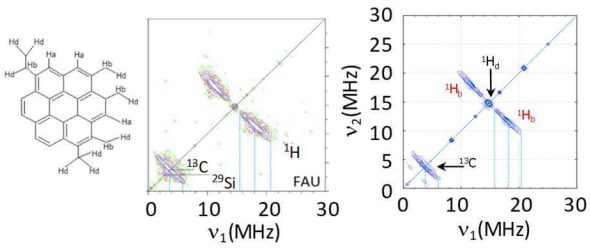

Figure 7: HYSCORE spectra of a specific coke trapped in a zeolite[13] compared to the HYSCORE spectra of nascent soot.

These similarities between the two HSYCORE spectra suggest that radicals in nascent soot are compatible with aromatic species roughly the size of coronene linked by short and branched aliphatic chains. This data is in good agreement with the previous work of Commodo et al.[3], in which the authors conclude that the core of nascent soot particles was mainly constituted of polyaromatic units having size of the order of 1 nm.

Conclusion

The analysis of the EEM determined from the flame carried out by means of EEM of pure PAHs first allowed the identification of a type of intermediate species between gaseous PAHs and solid soot particles characterized by optical properties distinct from PAHs and soot. In complement, EPR experiments provide experimental evidence of the presence in nascent soot of persistent aromatic radicals highly substituted by short aliphatic chains. The structure of these radicals appears consistent with resonance-stabilized π-radicals of the size of coronene. Our experimental data highlight that these radicals, which are absent from the condensable gas before soot formation, are formed and are essentially present in nascent soot and completely disappear from mature soot. Finally, we show that the formation of these species highlights strong correlations with the species fluorescing in the visible in the flame and might therefore be correlated to these unexplained signals.

Acknowledgements

This work was supported by the Agence Nationale de la Recherche through the LABEX CAPPA (ANR-11-LABX-0005), the Agence de l'Environnement et De la Maîtrise de l'Energie ADEME, the Ministry of Higher Education and Research, Hauts de France Regional Council and European Regional Development Fund (ERDF) through the Contrat de Projets Etat Region (CPER CLIMIBIO). Financial supports from the CERLA and IR INFRANALYTICS CNRS FR2054 for conducting the pulse EPR analyses is greatly appreciated.

References

[1] R.F. Service, Study Fingers Soot as a Major Player in Global Warming, Science. 319 (2008) 1745–1745.

[2] H. Wang, Formation of nascent soot and other condensed-phase materials in flames, Proc. Combust. Inst. 33 (2011) 41–67.

[3] M. Commodo, G. De Falco, A. Bruno, C. Borriello, P. Minutolo, A. D'Anna, Physicochemical evolution of nascent soot particles in a laminar premixed flame: from nucleation to early growth, Combust. Flame. 162 (2015) 3854–3863.

[4] J.W. Martin, M. Salamanca, M. Kraft, Soot inception: Carbonaceous nanoparticle formation in flames, Prog. Energy Combust. Sci. 88 (2022) 100956.

[5] C. Irimiea, A. Faccinetto, Y. Carpentier, I.-K. Ortega, N. Nuns, E. Therssen, P. Desgroux, C. Focsa, A comprehensive protocol for chemical analysis of flame combustion emissions by secondary ion mass spectrometry, Rapid Commun. Mass Spectrom. 32 (2018) 1015–1025.

[6] X. Mercier, O. Carrivain, C. Irimiea, A. Faccinetto, E. Therssen, Dimers of polycyclic aromatic hydrocarbons: the missing pieces in the soot formation process, Phys. Chem. Chem. Phys. 21 (2019) 8282–8294.

[7] F.J. Bauer, M.U.J. Degenkolb, F.J.T. Huber, S. Will, In situ characterisation of absorbing species in stationary premixed flat flames using UV–Vis absorption spectroscopy, Appl. Phys. B. 127 (2021) 115.

[8] T.W. Schmidt, The electronic spectroscopy of resonance-stabilised hydrocarbon radicals, Int. Rev. Phys. Chem. 35 (2016) 209–242.

[9] D. Gourier, O. Delpoux, L. Binet, H. Vezin, Nuclear Magnetic Biosignatures in the Carbonaceous Matter of Ancient Cherts: Comparison with Carbonaceous Meteorites, Astrobiology. 13 (2013) 932–947.

[10] D. Gourier, F. Robert, O. Delpoux, L. Binet, H. Vezin, A. Moissette, S. Derenne, Extreme deuterium enrichment of organic radicals in the Orgueil meteorite: Revisiting the interstellar interpretation?, Geochim. Cosmochim. Acta. 72 (2008) 1914–1923. https://doi.org/10.1016/j.gca.2008.01.017.

[11] A. Gardinier, S. Derenne, F. Robert, F. Behar, C. Largeau, J. Maquet, Solid state CP/MAS 13C NMR of the insoluble organic matter of the Orgueil and Murchison meteorites: quantitative study, Earth Planet. Sci. Lett. 184 (2000) 9–21.

[12] G.D. Cody, C.M.O. 'D. Alexander, NMR studies of chemical structural variation of insoluble organic matter from different carbonaceous chondrite groups, Geochim. Cosmochim. Acta. 69 (2005) 1085–1097.

[13] K. Ben Tayeb, S. Hamieh, C. Canaff, H. Nguyen, H. Vezin, L. Pinard, The radical internal coke structure as a fingerprint of the zeolite framework, Microporous Mesoporous Mater. 289 (2019) 109617.